Theoretical Considerations of Panel Flutter at High Supersonic Mach Numbers

JOHN DUGUNDJI*
Massachusetts Institute of Technology, Cambridge, Mass.

The general characteristics of panel flutter at high supersonic Mach numbers are examined theoretically. Linear plate theory and two-dimensional first-order aerodynamics are used. The paper attempts to clarify the important role of damping, the relationship between traveling and standing wave theories of panel flutter, and the effects of edge conditions. The solution procedures and general mathematical behavior may be of interest in other stability problems characterized by the appearance of complex eigenvalues.

Nomenclature

A = coefficient of basic Eq. (15)
A.R. = amplification ratio
a = length of panel
B_R, B_I = coefficients of basic Eq. (15)
b = width of panel
C = coefficient of basic Eq. (15)
c = wave speed
c_0 = reference wave speed $= 1.90\, c_M(h/b)$
c_A, c_M = speed of sound in air and in panel material
D = plate rigidity $= Eh^3/12(1-\nu^2)$
E_n = coefficient defined by Eq. (43)
f = factor defined by Eq. (50)
G_s = panel structural damping
g_A = aerodynamic damping coefficient $= 0.335\,\{M(M^2-2)/(M^2-1)^{3/2}\}(\rho_A/\rho_M)(c_A/c_M)(a/h)^2$
g_S = effective structural damping coefficient $= g_i\omega_i/\omega_0$
g_T = total damping coefficient $= g_A + g_S$
g_i = actual structural damping coefficient of ith mode $\approx 2 \times$ (critical damping ratio)
h = thickness of panel
i = $(-1)^{1/2}$
K = elastic foundation stiffness
k = foundation parameter $= Ka^4/\pi^4 D$
l = wavelength
M = Mach number
m = number of half-waves in lateral direction
N_x, N_y = longitudinal and lateral compressive forces
Δp_A = aerodynamic pressure loading
Q_R, Q_I = coefficients defined by Eqs. (23a) and (23b)
q_n = generalized coordinate of nth mode
r_x = longitudinal compression parameter $= N_x a^2/\pi^2 D$
S = parameter defined by Eq. (33)
t = time
U = velocity
$w, \bar{w}$ = deflection of panel
x, y = coordinates along length and width
z_m = roots of characteristic equation of Eq. (15)
$\bar{\alpha}$ = decay rate $= Re\{\bar{\theta}\}$
Δ = determinant defined by Eq. (20)
η = nondimensional coordinate $= y/b$
$\bar{\theta}$ = response of system $= \bar{\alpha} + i\bar{\omega}$
λ = dynamic pressure parameter $= \rho_A U^2 a^3/D(M^2-1)^{1/2}$
ν = Poisson's ratio ≈ 0.3
ξ = nondimensional coordinate $= x/a$
ρ_A, ρ_M = density of air and of panel material
τ = nondimensional time $= \omega_0 t$
Φ = complex function defined by Eq. (21)
ψ = effective structural damping ratio $= g_2\omega_2/g_1\omega_1$
ω = frequency
ω_0 = reference frequency $= \pi^2[D/\rho_M h a^4]^{1/2}$
ω_i = frequency of ith mode
$\bar{\omega}$ = nondimensional frequency $= \omega/\omega_0 = Im\{\bar{\theta}\}$

Subscripts

R = real
I = imaginary
F = flutter

Superscript

$\sim$ = corresponding nondimensional quantities for low-aspect-ratio panels (nondimensionalization based on b rather than on a)

Received November 15, 1965; revision received March 28, 1966. This work was supported by the Air Force Office of Scientific Research under Contract AF 49(638)-1528. The author wishes to acknowledge helpful discussions with Earl Dowell and the valuable computational assistance of Nancy Ghareeb.

* Associate Professor, Department of Aeronautics and Astronautics. Member AIAA.

1. Introduction

PANEL flutter is the self-excited oscillation of the external skin of a flight vehicle when exposed to an airflow on one side. This type of aeroelastic instability has received much study during the past 15 years, both theoretically and experimentally. The early work of Sylvester and Baker,[1] Nelson and Cunningham,[2] Fung,[3] Hedgepeth,[4] Movchan,[5] and Houbolt,[6] to mention a few names, has been supplemented by much recent work on the subject (see, for example, Refs. 7–14). Today, a great quantity of literature on panel flutter exists, and the problem is reasonably understood, although work still remains to be done to better correlate theory with experiment for certain panel configurations and Mach numbers. Fung,[10,15] in two excellent survey papers, discusses the status of the panel flutter problem. See also Dowell and Voss,[11] Bohon and Dixon,[14] Johns,[16] Kordes, Tuovila, and Guy,[17] and Shirk and Olsen.[18]

The present article will review the theoretical characteristics of panel flutter at high supersonic Mach numbers and will attempt to clarify some of the loose ends in the literature regarding the role of damping, traveling-wave vs standing-wave theories, and effects of edge conditions. It is hoped thereby to present clearly the high Mach number panel flutter problem and its ramifications, some of which may not have been apparent heretofore. The present article is a condensation of a longer report by the author.[19]

2. Basic Panel Flutter Equation and Its Solution

Consider a flat, rectangular panel, simply supported on all four edges and subject to a supersonic flow over one side (see Fig. 1). The panel additionally is subjected to midplane compressive forces N_x and N_y, rests on an elastic foundation K, and has a structural damping G_s. The governing differtial equation for this situation is

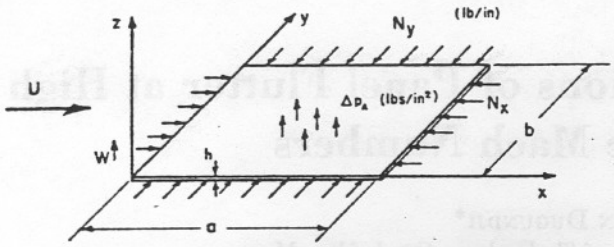

Fig. 1 Basic panel configuration. Panel rests on elastic foundation K (lb/in.³) and has viscous structural damping G_s (lb-sec/in.²).

$$D\nabla^4 w = \Delta p_A - \rho_M h \frac{\partial^2 w}{\partial t^2} - N_x \frac{\partial^2 w}{\partial x^2} - N_y \frac{\partial^2 w}{\partial y^2} - Kw - G_s \frac{\partial w}{\partial t} \quad (1)$$

The aerodynamic pressure for high supersonic Mach numbers ($M > 1.7$) can be reasonably described by two-dimensional, first-order theory approximations[2,3]:

$$\Delta p_A \approx -[\rho_A U^2/(M^2-1)^{1/2}] \times [(\partial w/\partial x) + (1/U)(\partial w/\partial t)(M^2-2)/(M^2-1)] \quad (2)$$

This assumes that the pressure on the bottom side remains at the freestream value p_∞.

Combining Eqs. (1) and (2) and introducing nondimensional coordinates ξ, η, τ results in the basic partial differential equation for panel flutter:

$$\frac{\partial^4 w}{\partial \xi^4} + 2\left(\frac{a}{b}\right)^2 \frac{\partial^4 w}{\partial \xi^2 \partial \eta^2} + \left(\frac{a}{b}\right)^4 \frac{\partial^4 w}{\partial \eta^4} + \lambda \frac{\partial w}{\partial \xi} + \pi^4 g_T \frac{\partial w}{\partial \tau} + \pi^4 \frac{\partial^2 w}{\partial \tau^2} + \pi^4 k w + \pi^2 r_x \frac{\partial^2 w}{\partial \xi^2} + \pi^2 r_y \left(\frac{a}{b}\right)^2 \frac{\partial^2 w}{\partial \eta^2} = 0 \quad (3)$$

where the following nondimensional parameters have been introduced:

$$\lambda = \rho_A U^2 a^3/D(M^2-1)^{1/2} \quad \text{(dynamic pressure parameter)} \quad (4)$$

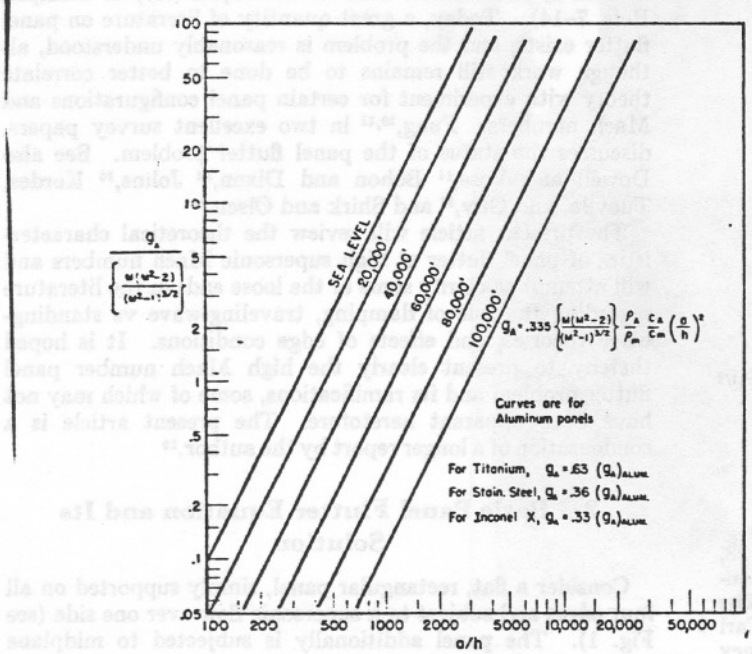

Fig. 2 Magnitude of aerodynamic damping.

$$g_T = g_A + g_S \quad \text{(total damping coefficient)} \quad (5)$$

$$g_A = 0.335\{M(M^2-2)/(M^2-1)^{3/2}\} \times (\rho_A/\rho_M)(c_A/c_M)(a/h)^2 \quad \text{(aerodynamic damping coefficient)} \quad (6)$$

$$g_S = g_i\omega_i/\omega_0 \quad \text{(effective structural damping coefficient)} \quad (7)$$

$$a/b \quad \text{(aspect ratio)} \quad (8)$$

$$k = Ka^4/\pi^4 D \quad \text{(foundation parameter)} \quad (9)$$

$$r_x = N_x a^2/\pi^2 D \quad \text{(longitudinal compression parameter)} \quad (10)$$

$$r_y = N_y a^2/\pi^2 D \quad \text{(lateral compression parameter)} \quad (11)$$

In the foregoing, the reference frequency ω_0 represents the lowest natural frequency of a two-dimensional simply supported panel ($a/b \to 0$) with no airflow, elastic foundation, or midplane compressive forces present. Also, the total damping coefficient g_T is the sum of an aerodynamic damping coefficient g_A and an effective structural damping coefficient g_S. The g_A, first introduced by Houbolt,[6] is shown in Fig. 2 for different panel sizes, altitudes, and panel materials.† The g_S is a consequence of the assumed constant structural damping G_s, which can be expressed as

$$G_s = g_i\omega_i\rho_M h \quad (12)$$

where $g_i = 2\zeta_i = 2 \times$ (critical damping ratio) of any mode ω_i. The form of Eq. (12) implies that, for any other mode ω_j, the actual structural damping coefficient g_j will be given by $g_j = g_i\omega_i/\omega_j$. For typical panels, g_i ranges from 0 to 0.03 approximately. The consequences of using other values of g_j for the higher modes is explored in Sec. 5.

The basic partial differential equation for panel f[illegible], Eq. (3), is solved subject to the simply supported boun[illegible]y conditions:

$$\text{at} \quad \xi = 0, \quad 1 \to w = 0, \quad \partial^2 w/\partial \xi^2 = 0 \quad (13a)$$

$$\text{at} \quad \eta = 0, \quad 1 \to w = 0, \quad \partial^2 w/\partial \eta^2 = 0 \quad (13b)$$

The solution procedure begins by seeking solutions in the form

$$w(\xi, \eta, \tau) = \bar{w}(\xi)[\sin m\pi\eta]e^{\bar{\theta}\tau} \quad (14)$$

where, in general, $\bar{\theta} = \bar{\alpha} + i\bar{\omega}$. Placing Eq. (14) into Eq. (3) yields the ordinary differential equation

$$\frac{d^4\bar{w}}{d\xi^4} + C\frac{d^2\bar{w}}{d\xi^2} + A\frac{d\bar{w}}{d\xi} + (B_R + iB_I)\bar{w} = 0 \quad (15)$$

where

$$C = \pi^2[-2(ma/b)^2 + r_x] \quad (16)$$

$$A = \lambda \quad (17)$$

$$B_R + iB_I = \pi^4[(ma/b)^4 + k - (ma/b)^2 r_y + g_T\bar{\theta} + \bar{\theta}^2] \quad (18)$$

This ordinary differential equation, Eq. (15), subject to the boundary conditions, Eq. (13a), is now solved thoroughly. The general solution of Eq. (15) is

$$\bar{w}(\xi) = c_1 e^{z_1\xi} + c_2 e^{z_2\xi} + c_3 e^{z_3\xi} + c_4 e^{z_4\xi} \quad (19)$$

where the c_m are arbitrary complex constants, and the [illegible]e the four roots of the complex characteristic equation [illegible]d. (15). Upon inserting $\bar{w}$ into the boundary conditions, Eq.

† The Mach number factor in braces is often assumed to be its aerodynamic piston theory value of 1. See Ashley and Zartarian.[20]

(13a), the following determinant Δ must equal zero for nontrivial solutions:

$$\Delta = \begin{vmatrix} 1 & 1 & 1 & 1 \\ z_1^2 & z_2^2 & z_3^2 & z_4^2 \\ e^{z_1} & e^{z_2} & e^{z_3} & e^{z_4} \\ z_1^2 e^{z_1} & z_2^2 e^{z_2} & z_3^2 e^{z_3} & z_4^2 e^{z_4} \end{vmatrix} = 0 \tag{20}$$

For a given C and A, various values of B_R and B_I are selected, and the four roots z_1, z_2, z_3, z_4 are found. Then the complex function Φ is evaluated, where‡

$$\Phi = \Delta/(z_1 - z_2)(z_1 - z_3)(z_1 - z_4)(z_2 - z_3)(z_2 - z_4)(z_3 - z_4) \tag{21}$$

The combination of B_R and B_I which makes $\Phi(B_R, B_I) = 0$ is a solution (eigenvalue) of Eqs. (15) and (13a) for the given C, A combination.

Equations (15) and (13a) were solved numerically by an IBM 1620 computer. Since many eigenvalues B_R, B_I can be found for each C, A combination, it was necessary to trace out continuously the proper eigenvalue branch by increasing A continuously from zero for a fixed value of C. For low values of A, the eigenvalues are real ($B_I = 0$), but above a certain value of A, they become complex ($B_I \neq 0$). Figures 3a and 3b show the real eigenvalues ($B_I = 0$), whereas Figs. 4a–4c show the complex eigenvalues. Only the most critical eigenvalue branches for this problem are indicated (largest B_I for a given C, A combination).

It remains to relate the general coefficients C, A, B_R, B_I to the pertinent physical parameters λ, g_T, a/b, k, r_x, r_y, $\bar{\theta}$ of the problem.§ It is convenient to rewrite Eq. (18) as

$$\bar{\theta}^2 + g_T\bar{\theta} - (Q_R + iQ_I) = 0 \tag{22}$$

where

$$Q_R = B_R/\pi^4 - (ma/b)^4 - k + (ma/b)^2 r_y \tag{23a}$$

$$Q_I = B_I/\pi^4 \tag{23b}$$

Equation (22) can be solved for $\bar{\theta}$ to give

$$\bar{\theta} = [-g_T/2 + Re\{(\Gamma)^{1/2}\}] + i[Im\{(\Gamma)^{1/2}\}] \tag{24}$$

where

$$Re\{(\Gamma)^{1/2}\} = \pm[1/(2)^{1/2}](+\{[(g_T/2)^2 + Q_R]^2 + [Q_I]^2\}^{1/2} + (g_T/2)^2 + Q_R)^{1/2} \tag{25a}$$

$$Im\{(\Gamma)^{1/2}\} = Q_I/2\, Re\{(\Gamma)^{1/2}\} \tag{25b}$$

For a configuration defined by given values of λ, g_T, a/b, k, r_x, and r_y, Eqs. (16) and (17) are used to find C and A. From the appropriate Figs. 3 and 4, values of B_R and B_I are found. Then Q_R and Q_I are evaluated from Eqs. (23a) and (23b). Finally, $\bar{\theta} = \bar{\alpha} + i\bar{\omega}$ is solved from Eqs. (24, 25a, and 25b).

The complete panel behavior is characterized by plotting the $\bar{\alpha} + i\bar{\omega}$ variation with increasing dynamic pressure λ. Instability occurs when $\bar{\alpha}$ becomes positive (static type if also $\bar{\omega} = 0$, dynamic type if also $\bar{\omega} \neq 0$). Some typical plots are shown in Fig. 5. For the case of no damping, $g_T = 0$, instability does not set in until after two undamped natural frequencies have merged (hence, the term "frequency coalescence flutter"). For some damping present, $g_T > 0$, the instability sets in at a somewhat higher value of λ. This occurs when $\bar{\alpha} = 0$ in Eq. (24). By routine algebraic manipulation, this flutter condition occurs at the value of λ when

$$Q_I/(-Q_R)^{1/2} = g_T \tag{26}$$

‡ The function Φ, rather than Δ itself, is evaluated to prevent repeated roots from causing the determinant to approach zero. Also, Φ, unlike the Δ, will preserve its sign if one replaces z_1 by z_2, etc.

§ The mode parameter m is taken as $m = 1$. Actually, all results come out in terms of an effective aspect ratio ma/b.

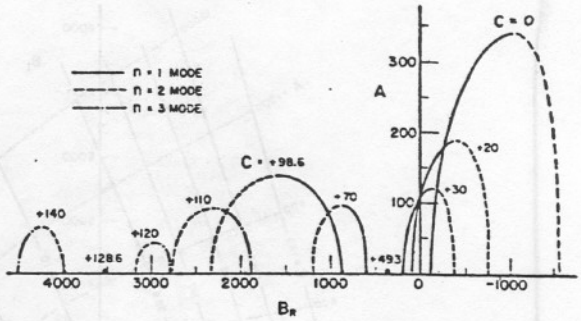

C	B_R FOR A = 0			
	n = 1	n = 2	n = 3	n = 4
0	-97	-1560	-7870	-24,900
30	199	-373	-5210	-20,200
49.3	388	388	-3500	-17,100
70	593	1200	-1660	-13,800
98.6	874	2330	874	-9,320
110	987	2780	1880	-7,530
120	1090	3170	2770	-5,950
128.6	1170	3520	3520	-4,590
140	1280	3960	4550	-2,790

a)

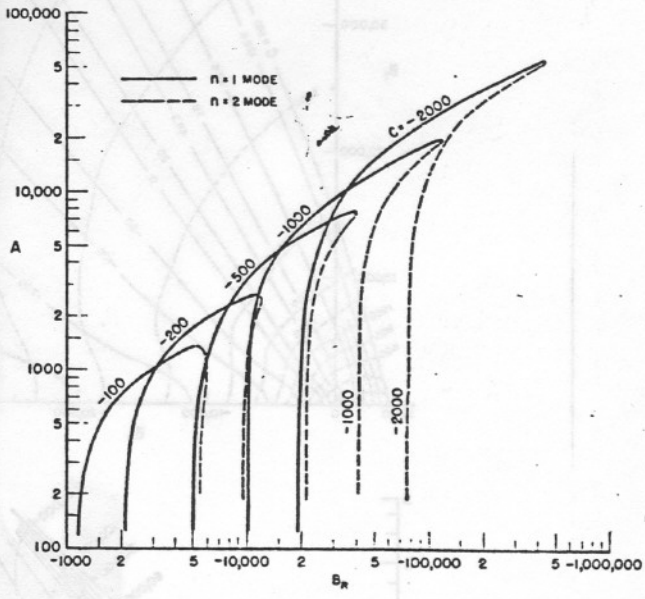

b)

Fig. 3 Real eigenvalues ($B_I = 0$ case).

At this flutter condition, the corresponding flutter frequency is

$$\bar{\omega}_F = (-Q_R)^{1/2} = \omega_F/\omega_0 \tag{27}$$

Frequently, only the flutter condition is determined. However, the violence of the flutter can also be obtained from Eq. (24).

The deflection shape $w(\xi, \eta, \tau)$ for any physical situation is found from real part of the right-hand side of Eq. (14). The $w(\xi)$ is given by Eq. (19), where the roots z_m are those for the given situation, and the complex constants c_m are found from the boundary conditions, Eq. (15a). This results in

$$w(\xi, \eta, \tau) = [\sin m\pi\eta]e^{\bar{\alpha}\tau}(\bar{w}_R \cos\bar{\omega}\tau - \bar{w}_I \sin\bar{\omega}\tau) \tag{28}$$

This can be plotted for various times during one cycle ($\bar{\omega}\tau = 2\pi$) to give a clear physical picture of the deflection shape.

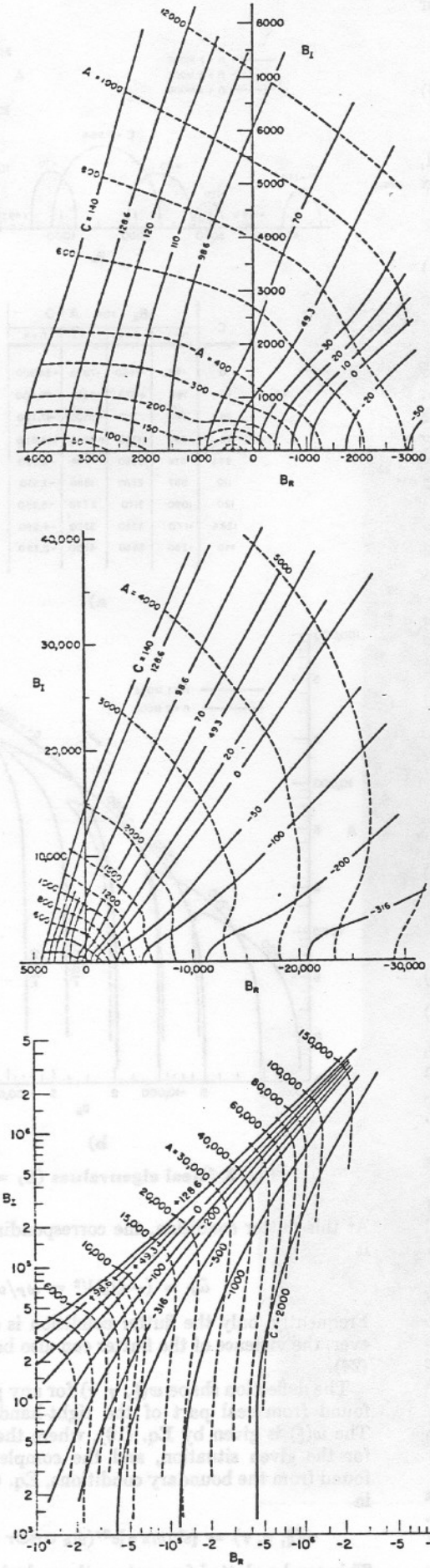

Fig. 4 Complex eigenvalues.

Some deflection shapes at flutter conditions ($\bar{\alpha} = 0$) are given in Figs. 6a–6h for various C, A combinations and the most critical eigenvalue branch (largest B_I for this given C, A combination). For $A = 0$, the deflection shapes are simple sine shape standing-wave types. As the coefficient A is increased for a fixed C, the deflection shape changes from a standing-wave type at low values of A, where purely real eigenvalues ($B_I = 0$) are present, to a traveling-wave type at high values of A, where complex eigenvalues ($B_I \neq 0$) are present.

The solution procedures used here represent an exact solution rather than a modal solution of the differential equation and hence do not possess convergence difficulties. These procedures are analogous to those used previously by Dugundji and Ghareeb[21] for solving a related differential equation (see also Movchan[5,22]).

3. Applications

The general theory presented in Sec. 2 is applied to various physical panel configurations. Generally, only the flutter condition ($\bar{\alpha} = 0$) will be examined, but an example of the complete panel behavior will also be given.

a. Pure Aspect-Ratio Effects, a/b

For this series of panels, one considers $k = r_x = r_y = 0$. Here, only dynamic-type instability is possible. Figure 7 shows the dynamic pressure parameter at flutter λ_F vs damping coefficient g_T for different aspect ratios a/b. The λ_F becomes large for low aspect ratios (high a/b). Also, λ_F becomes independent of g_T at low values of g_T and roughly proportional to g_T at high values of g_T. This indicates a change of panel flutter from a constant dynamic pressure phenomenon at low values of damping to a constant velocity phenomenon at high values of damping (thin panels in dense air). This also permits one to use the "static airforce approximation"[4] for $g_T < 1$.

The flutter frequencies $\bar{\omega}_F$ are indicated in Fig. 7. The deflection mode shapes for the point marked with a heavy dot are given by Figs. 6a–6c ($a/b = 0$; $\lambda_F = 370$, 2000, 20,000) and Fig. 6e ($a/b = 10$; $\lambda_F = 60{,}000$). The modes are seen to change from standing-wave types at low values of g_T to traveling-wave types at high values of g_T. Also, the modes become of very short wavelength, the deflections tend to be concentrated at the rear end, and the flutter frequency becomes high at large values of g_T and low aspect ratios (high

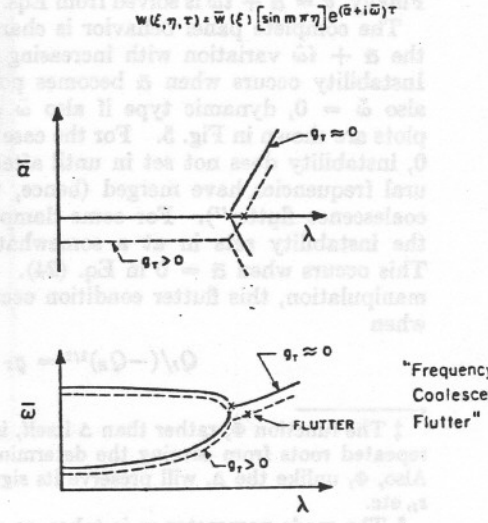

Fig. 5 Typical plots of panel behavior.

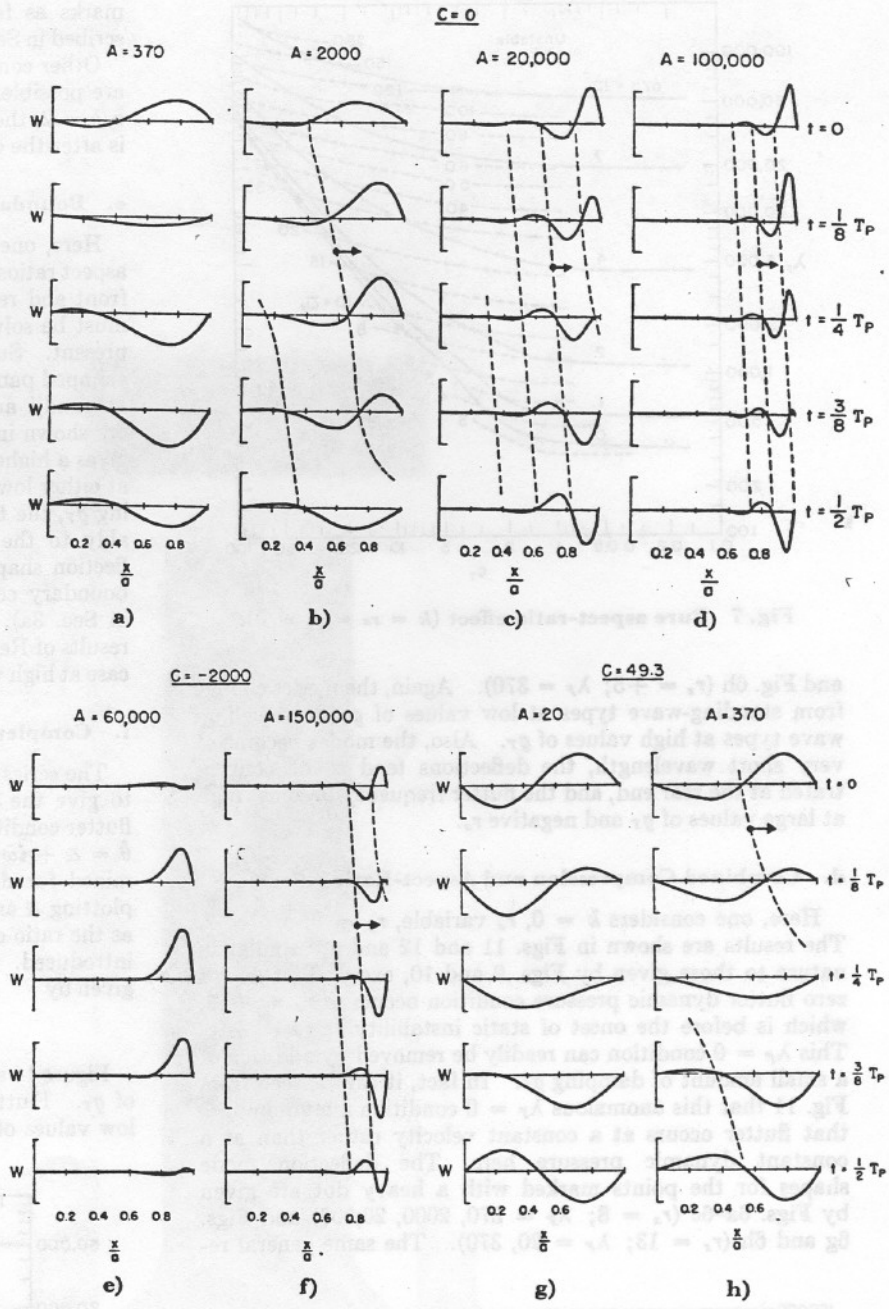

Fig. 6 Mode shapes.

a/b). The first-order aerodynamics equation (2) may be somewhat inaccurate at the higher $\bar{\omega}_F$'s.

b. Pure Elastic Foundation Effect, k

Here, one considers $a/b = r_x = r_y = 0$. Only dynamic instability is possible. Figure 8 shows λ_F vs g_T for different elastic foundation parameters k. The λ_F increases with g_T and with k. The presence of small damping g_T is important at high values of k, since it raises λ_F well above the $g_T = 0$ value of $\lambda_F = 343$. Again, the flutter phenomenon changes toward a constant velocity rather than a constant dynamic pressure phenomenon as g_T or k becomes large.

The flutter frequencies $\bar{\omega}_F$ are indicated in Fig. 8. At high values of k, the $\bar{\omega}_F$ becomes the simple natural frequency of the section mass-on-spring foundation. The deflection mode shapes for the points marked with heavy dots are given by Figs. 6a–6c (any value of k; $\lambda_F = 370, 2000, 20{,}000$). Again, the modes change from standing-wave types at low values of g_T and k to traveling-wave types at high values of g_T and k. Also, the modes become of very short wavelength, the deflections tend to be concentrated at the rear end, and the flutter frequency becomes high at large values of g_T and k.

c. Pure Longitudinal Compression Effect, r_x

Here, one considers $a/b = k = r_y = 0$. Figure 9 shows λ_F vs g_T for different longitudinal compression forces r_x. The λ_F increases with increasing tension (negative r_x) and also with increasing damping g_T. Again, the flutter phenomenon changes toward a constant velocity rather than a constant dynamic pressure phenomenon as g_T becomes large. For compressive forces $r_x > +1$, static instability may also occur. The nature of these curves for positive r_x is better illustrated by a cross plot, Fig. 10, which shows λ for instability plotted vs r_x. The regions of dynamic and static instability are readily apparent here. The point $\lambda = 0$, $r_x = 1$ represents the Euler buckling load of the panel. The aerodynamic forces may stabilize an otherwise statically unstable panel.

The flutter frequencies $\bar{\omega}_F$ are indicated in Fig. 10. The deflection mode shapes for the points marked with a heavy dot are given by Figs. 6a–6c ($r_x = 0$; $\lambda_F = 370, 2000, 20{,}000$)

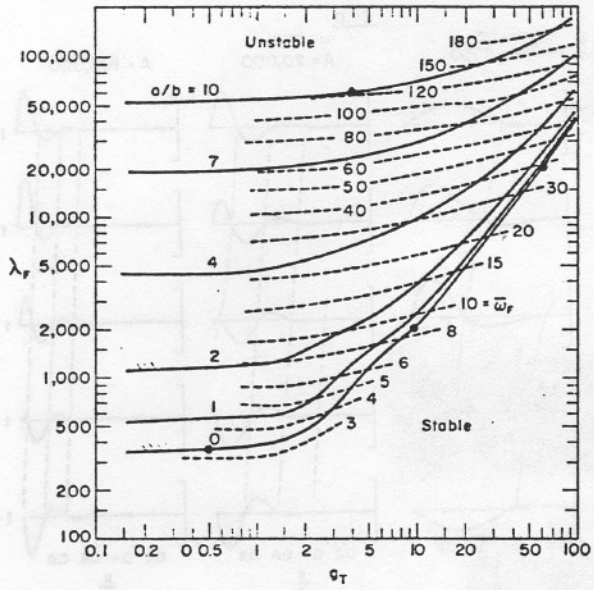

Fig. 7 Pure aspect-ratio effect ($k = r_x = r_y = 0$).

and Fig. 6h ($r_x = +5$; $\lambda_F = 370$). Again, the modes change from standing-wave types at low values of g_T to traveling-wave types at high values of g_T. Also, the modes become of very short wavelength, the deflections tend to be concentrated at the rear end, and the flutter frequency becomes high at large values of g_T and negative r_x.

d. Combined Compression and Aspect-Ratio Effects

Here, one considers $k = 0$, r_x variable, $r_y = 0$, $a/b = 2$. The results are shown in Figs. 11 and 12 and are similar in nature to those given by Figs. 9 and 10, except that now a zero flutter dynamic pressure condition occurs at $r_x = +13$, which is before the onset of static instability at $r_x = +16$. This $\lambda_F = 0$ condition can readily be removed by addition of a small amount of damping g_T. In fact, it can be seen from Fig. 11 that this anomalous $\lambda_F = 0$ condition merely implies that flutter occurs at a constant velocity rather than at a constant dynamic pressure here. The deflection mode shapes for the points marked with a heavy dot are given by Figs. 6a–6c ($r_x = 8$; $\lambda_F = 370, 2000, 20{,}000$) and Figs. 6g and 6h ($r_x = 13$; $\lambda_F = 20, 370$). The same general remarks as for the pure longitudinal compression effect described in Sec. 3c apply here.

Other combinations of compression and aspect-ratio effects are possible. For example, for $k = 0$, r_x variable, $r_y = r_x$, $a/b = 2$, the $\lambda_F = 0$ condition will occur at $r_x = +13$, which is after the onset of static instability at $r_x = +5$.

e. Boundary Support Effect

Here, one considers $k = r_x = r_y = 0$, but with different aspect ratios and different boundary support conditions on the front and rear edges of the panel. The basic equation (18) must be solved subject to the different boundary conditions present. Such calculations were performed for clamped-clamped panels by Movchan[23] and for clamped-free panels by Dugundji and Ghareeb.[21] The resulting plots of λ_F vs g_T are shown in Fig. 13. In general, the clamped-clamped case gives a higher λ_F than the simply supported case. However, at either low aspect ratios (high a/b) or high values of damping g_T, the two λ_F's approach each other. This is due probably to the shorter wavelengths present in the flutter deflection shapes here and, hence, a lesser influence of the end boundary conditions (see flutter deflection shape discussion in Sec. 3a). Also shown is a clamped-free beam from the results of Ref. 21, which also approaches the simply supported case at high values of g_T.

f. Complete Panel Behavior

The series of panels examined in Sec. 3a was reinvestigated to give the complete panel behavior instead of merely the flutter condition. Here, $k = r_x = r_y = 0$. The variation of $\bar{\theta} = \bar{\alpha} + i\bar{\omega}$ vs the dynamic pressure parameter λ was determined for different a/b and g_T configurations. Instead of plotting $\bar{\alpha}$ and $\bar{\omega}$ vs λ, the amplification ratio (A.R.) defined as the ratio of amplitudes during one cycle of oscillation is introduced. This indicates the violence of flutter and is given by

$$\text{A.R.} = e^{2\pi\bar{\alpha}/\bar{\omega}} \tag{29}$$

Figure 14 shows A.R. vs λ for $a/b = 0, 4$ and several values of g_T. Flutter (A.R. > 1) sets in sharply for $a/b = 0$ and low values of damping g_T. For low aspect ratios ($a/b =$

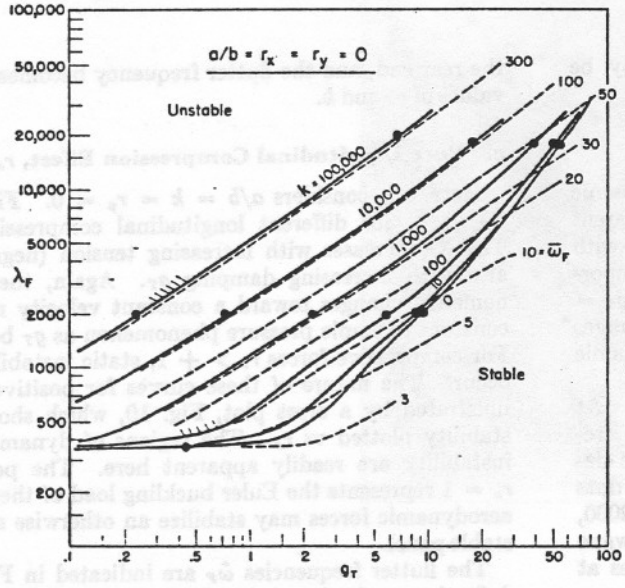

Fig. 8 Pure spring effect.

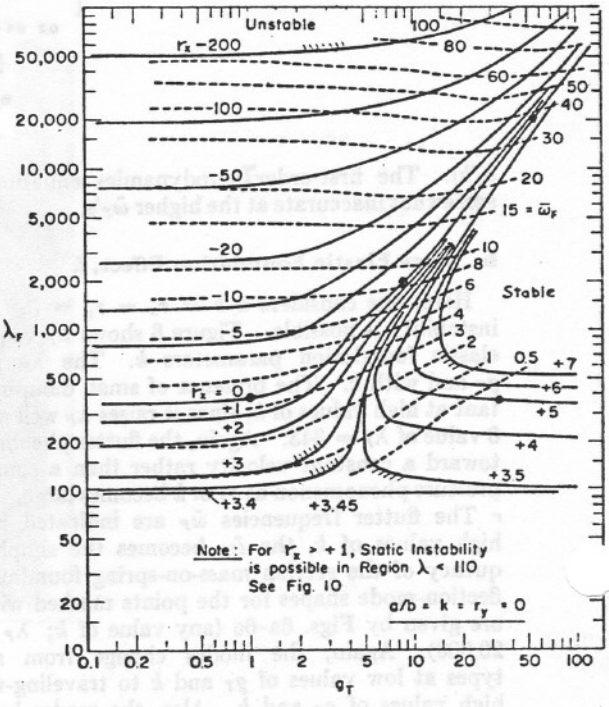

Fig. 9 Pure longitudinal compression effect.

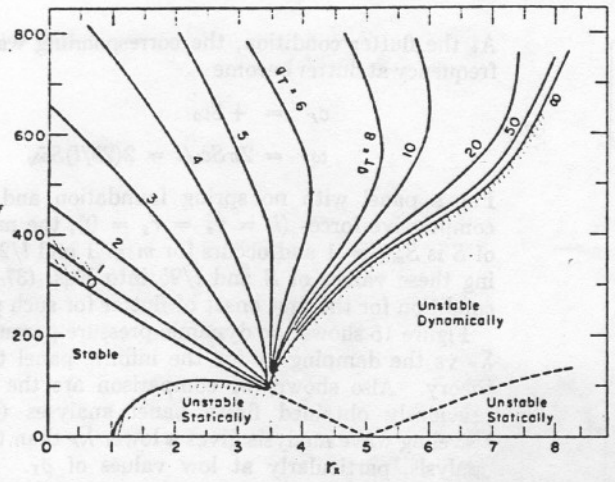

Fig. 10 Pure longitudinal compression effect (cross plot) ($a/b = k = r_y = 0$).

and also for high values of g_T, the flutter condition comes in more mildly. Also shown are some values of the frequency $\bar{\omega}$ associated with these amplification ratios. The first-order aerodynamics equation (2) may be somewhat inaccurate at the high $\bar{\omega}$'s.

4. Traveling Wave Analysis

One might consider a low-aspect-ratio panel as an infinitely long strip of finite width b and seek traveling wave solutions of the basic partial differential equation.¶ Although the use of first-order aerodynamics, Eq. (2), has certain limitations when applied to traveling waves,[23] it will be used anyway to assess the differences between the traveling wave analysis and the finite panel analysis of the same mathematical equation.

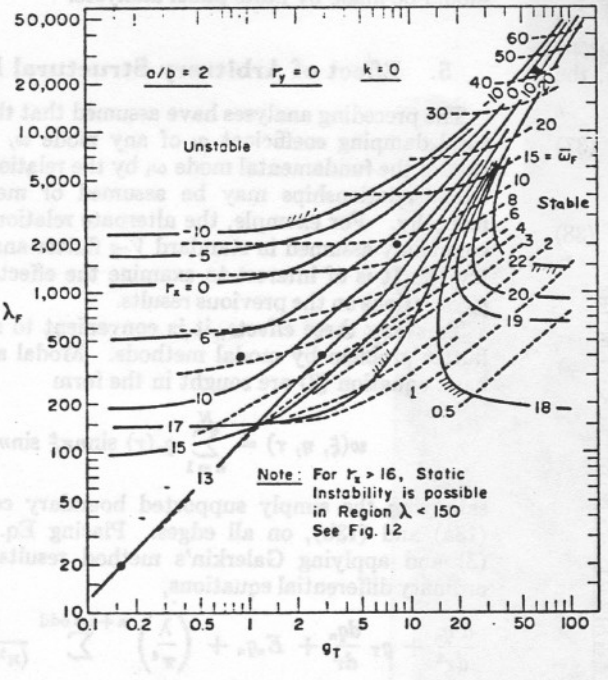

Fig. 11 Combined compression and aspect-ratio effect.

¶ This traveling wave approach for low-aspect-ratio panels was investigated by Dowell[24] using the complete linearized aerodynamic theory. Also, this traveling wave approach is often used in problems of cylindrical shell flutter.[10]

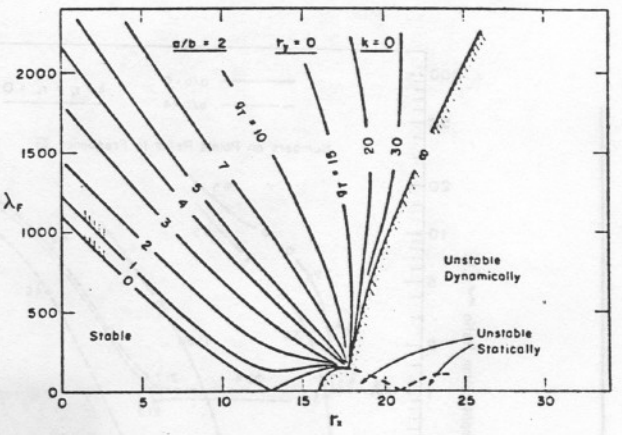

Fig. 12 Combined compression and aspect-ratio effect (cross plot).

Combining the governing differential equations (1) and (2) and introducing new nondimensional coordinates ξ, η, $\bar{\tau}$ results in the alternate partial differential equation for panel flutter:

$$\frac{\partial^4 w}{\partial \xi^4} + 2\frac{\partial^4 w}{\partial \xi \partial \eta^2} + \frac{\partial^4 w}{\partial \eta^4} + \bar{\lambda}\frac{\partial w}{\partial \xi} + \pi^4 \bar{g}_T \frac{\partial w}{\partial \bar{\tau}} + \pi^4 \frac{\partial^2 w}{\partial \bar{\tau}^2} + \pi^4 \bar{k} w + \pi^2 \bar{r}_x \frac{\partial^2 w}{\partial \xi^2} + \pi^2 \bar{r}_y \frac{\partial^2 w}{\partial \eta^2} = 0 \quad (30)$$

where new nondimensional parameters have been introduced, λ, $\bar{g}_T$, $\bar{g}_A$, $\bar{g}_S$, $\bar{k}$, $\bar{r}_x$, $\bar{r}_y$. These are similar to Eqs. (4–11) except that now all nondimensionalizations are based solely on the width b.

Traveling wave solutions of Eq. (30) are sought in the form

$$w(\xi, \eta, \bar{\tau}) = w_0[\sin m\pi\eta]e^{i2\pi(ct-x)/l} \quad (31)$$

where l is the wavelength and c is the wave speed, which, in general, may be complex, i.e., $c = c_R + ic_I$. Placing Eq. (31) into Eq. (30) will yield the algebraic equation

$$(c/c_0)^2 - i(\bar{g}_T l/4b)(c/c_0) - S^2 + i(\bar{\lambda} l/8\pi^3 b) = 0 \quad (32)$$

where

$$S = \tfrac{1}{2}[m^4(l/2b)^2 + 2m^2 + 1/(l/2b)^2 + \bar{k}(l/2b)^2 - \bar{r}_x - m^2\bar{r}_y(l/2b)^2]^{1/2} \quad (33)$$

$$c_0 = 2b\bar{\omega}_0/\pi = 1.90\, c_M(h/b) \quad (34)$$

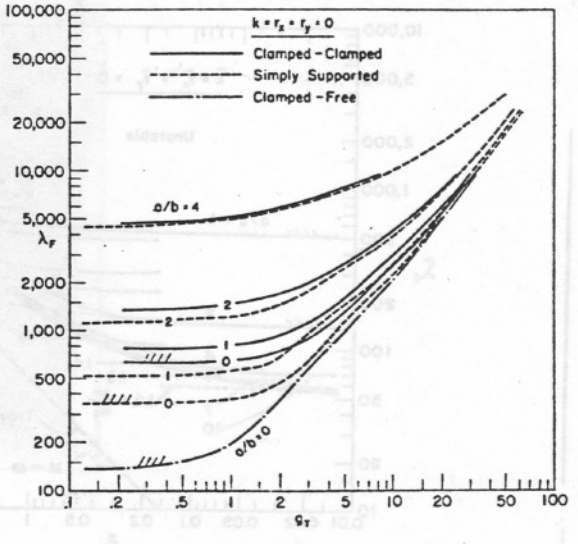

Fig. 13 Boundary support effect.

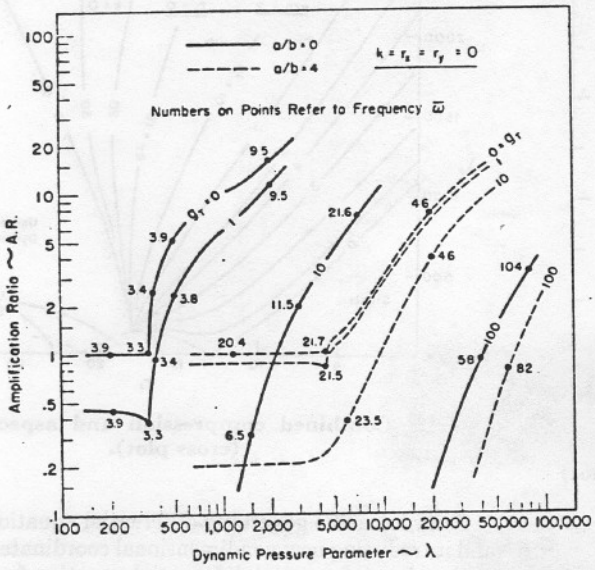

Fig. 14 Amplification ratio vs dynamic pressure parameter.

The reference wave speed c_0 can be interpreted physically as the minimum vacuum wave speed possible for a panel with $k = r_x = r_y = 0$.

Solving Eq. (32) for the wave speed c in the presence of air forces and damping gives

$$c/c_0 = [\mathrm{Re}\{(\Gamma)^{1/2}\}] + i[(\bar{g}_T l/8b) + Im\{(\Gamma)^{1/2}\}] \quad (35)$$

where

$$Re\{(\Gamma)^{1/2}\} = -(\bar{\lambda} l/16\pi^3 b)/Im\{(\Gamma)^{1/2}\} \quad (36a)$$

$$Im\{(\Gamma)^{1/2}\} = \pm[1/(2)^{1/2}](+\{[S^2 - (\bar{g}_T l/8b)^2]^2 + [\bar{\lambda} l/8\pi^3 b]^2\}^{1/2} - \{S^2 - (\bar{g}_T l/8b)^2\})^{1/2} \quad (36b)$$

The complete panel behavior is characterized by plotting the $c_R + ic_I$ variation with increasing dynamic pressure $\bar{\lambda}$ for various wavelengths $l/2b$. Instability is assumed to occur when c_I becomes negative. Using Eqs. (35) and (36b), the flutter condition ($c_I = 0$) can be shown to be

$$\bar{\lambda}_F = 2\pi^3 S \bar{g}_T \quad (37)$$

or, equivalently,

$$U_F = 1.90[(M^2 - 2)/(M^2 - 1)]Sc_M(h/b) \quad (38)$$

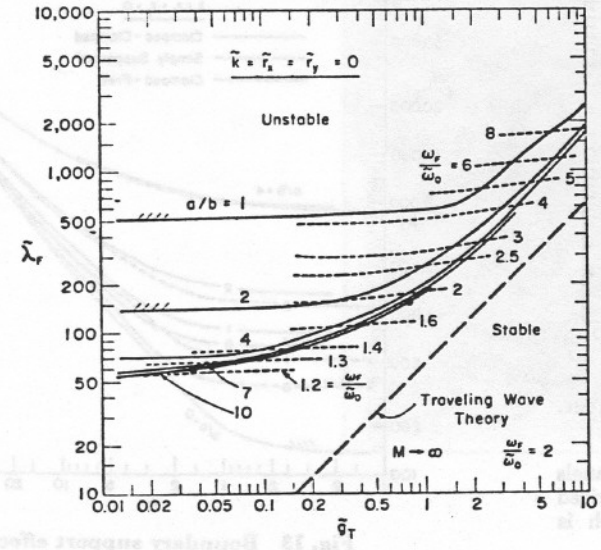

Fig. 15 Low-aspect-ratio effect.

At the flutter condition, the corresponding wave speed and frequency at flutter become

$$c_F = +Sc_0 \quad (39)$$

$$\omega_F = 2\pi S c_0/l = 2(2b/l)S\bar{\omega}_0 \quad (40)$$

For a panel with no spring foundation and no midplane compressive forces ($k = r_x = r_y = 0$), the minimum value of S is $S_{\min} = 1$ and occurs for $m = 1$ and $l/2b = 1$. Placing these values of S and $l/2b$ into Eqs. (37–40) gives the condition for the first onset of flutter for such panels.

Figure 15 shows the dynamic pressure parameter at flutter $\bar{\lambda}_F$ vs the damping $\bar{g}_T$ for the infinite panel traveling wave theory. Also shown for comparison are the results of the previously obtained finite panel analyses (Fig. 7). The traveling wave analysis gives a lower $\bar{\lambda}_F$ than the finite panel analysis, particularly at low values of $\bar{g}_T$. At the higher values of $\bar{g}_T$, the agreement and trends are better between the two theories. The flutter frequencies $\omega_F/\bar{\omega}_0$ are also indicated, and the agreements are fair. The deflection mode shapes for the traveling wave analysis are simple sine-shaped traveling waves of wavelength $l = 2b$, traveling at a wave speed $c = c_0$, and having a frequency $\omega_F = 2\omega_0$. The corresponding deflection mode shapes of the finite panel for the points marked by a heavy dot are given in Figs. 6e and 6f ($a/b = 10$; $\bar{g}_T = 0.036, 0.80$). They clearly resemble traveling waves and are qualitatively similar in wavelength, wave speed, and frequency to the infinite panel, particularly at high values of $\bar{g}_T$. These finite panels, though, show large deflection amplitudes toward the rear of the panel, as compared with the uniform deflection amplitudes of the infinite panel, traveling wave analysis.

Summarizing, it appears that an approximate idea of the flutter speed, frequency, wave speed, and wavelength can be obtained from an infinite panel, traveling wave analy[illegible] for long, narrow panels at high values of damping $\bar{g}_T$ (ligh[illegible] in panels in dense air). However, the end effects still play important roles for panels of $a/b = 10$, and any accurate estimation of the flutter characteristics and deflection shapes should be made by finite panel analyses.

5. Effect of Arbitrary Structural Damping

The preceding analyses have assumed that the actual structural damping coefficient g_j of any mode ω_j was related to that of the fundamental mode ω_1 by the relation $g_j = g_1\omega_1/\omega_j$. Other relationships may be assumed or measured experimentally. For example, the alternate relationship $g_j = g_1$ is commonly assumed in standard V-g flutter analyses in industry.** It is of interest to examine the effect of these other g_j variations on the previous results.

To study these effects, it is convenient to solve the panel flutter problem by modal methods. Modal solutions of the basic equation (3) are sought in the form

$$w(\xi, \eta, \tau) = \sum_{n=1}^{N} q_n(\tau) \sin n\pi\xi \sin m\pi\eta \quad (41)$$

satisfying the simply supported boundary conditions, Eqs. (13a) and (13b), on all edges. Placing Eq. (41) into Eq. (3) and applying Galerkin's method results in the set of ordinary differential equations,

$$\frac{d^2q_n}{d\tau^2} + g_T\frac{dq_n}{d\tau} + E_n q_n + \left(\frac{\lambda}{\pi^4}\right)^{n+s=\mathrm{odd}} \sum \frac{4sn}{(n^2 - s^2)} q_s = 0 \quad (42)$$

where

** This corresponds to structural damping of the form $+G_s\,\partial^3 w/\partial x^2\partial t$ rather than $-G_s\,\partial w/\partial t$ in Eq. (1) for the $a/b = k = r_x = r_y = 0$ panel studied subsequently.

$$E_n = n^4 + 2n^2(ma/b)^2 + (ma/b)^4 + k - r_x n^2 - r_y(ma/b)^2 \tag{43}$$

The foregoing summation is taken over all of the s terms for which $n + s$ is an odd integer.

Consider, for simplicity, a two-mode analysis. The preceding set of equations becomes

$$\begin{aligned}(d^2q_1/d\tau^2) + g_T(dq_1/d\tau) + E_1q_1 - (8\lambda/3\pi^4)q_2 &= 0\\ (d^2q_2/d\tau^2) + fg_T(dq_2/a\tau) + E_2q_2 + (8\lambda/3\pi^4)q_1 &= 0\end{aligned} \tag{44}$$

In the second equation, an arbitrary factor f was introduced to permit changing the amount of total damping g_T of the second mode. To investigate stability, one sets

$$q_n(\tau) = q_n e^{\bar{\theta}\tau} \tag{45}$$

and expands the determinant of the preceding equations to obtain the characteristic equation:

$$\bar{\theta}^4 + [g_T(1 + f)]\bar{\theta}^3 + [E_1 + E_2 + fg_T^2]\bar{\theta}^2 + [g_T(E_2 + fE_1)]\bar{\theta} + [E_1E_2 + (8\lambda/3\pi^4)^2] = 0 \tag{46}$$

The roots $\bar{\theta} = \bar{\alpha} + i\bar{\omega}$ of Eq. (46) are examined as λ increases from zero for any fixed configuration. This gives the complete panel behavior. To investigate only the flutter condition $\bar{\alpha} = 0$, one sets $\bar{\theta} = i\bar{\omega}_F$ in Eq. (46). Solving first the imaginary part and then the real part gives the flutter conditions

$$\bar{\omega}_F = \omega_F/\omega_0 = [(E_2 + fE_1)/(1 + f)]^{1/2} \tag{47}$$

$$\lambda_F = 18.26[2(f)^{1/2}/(1 + f)] \times [(E_2 - E_1)^2 + g_T^2(E_2 + fE_1)(1 + f)]^{1/2} \tag{48}$$

A similar equation for λ_F was presented by Bolotin.[9]

Returning to the damping characteristics, one differentiates between the damping in each mode,

$$\begin{aligned}g_{T1} &= g_A + g_{S1} = g_T\\ g_{T2} &= g_A + g_{S2} = fg_T\end{aligned} \tag{49}$$

where the effective structural damping coefficient g_{Si} of the ith mode is given from Eq. (7) as $g_{Si} = g_i\omega_i/\omega_0$. One may then express the factor f as

$$f = g_{T2}/g_{T1} = [1 + (g_{S1}/g_A)]/[1 + \psi(g_{S1}/g_A)] \tag{50}$$

Thus, f depends on two nondimensional ratios, namely,

$$g_{S1}/g_A = (g_1/g_A)(\omega_1/\omega_0) \tag{51}$$

$$\psi = g_{S2}/g_{S1} = (g_2\omega_2/g_1\omega_1) \tag{52}$$

Also, the total damping and the undamped natural frequencies of this two-mode system can be expressed as

$$g_T = g_A[1 + (g_{S1}/g_A)] \tag{53}$$

$$\omega_i/\omega_0 = [E_i]^{1/2} \tag{54}$$

For any combination of g_A, g_1, g_2, the ratios g_{S1}/g_A and ψ are first evaluated. The resulting values of f and g_T from Eqs. (50) and (53) may then be placed into Eq. (48) to obtain λ_F.

Figure 16 shows the factor f vs g_{S1}/g_A for various values of ψ. Also shown is the parameter $2(f)^{1/2}/(1 + f)$ vs f. For a given ψ, as g_{S1}/g_A increases from zero, the value of f varies from $f = 1$ to the asymptotic value $f = 1/\psi$. The corresponding value of $2(f)^{1/2}/(1 + f)$ decreases monotonically from unity to some other asymptotic value. Placing these results into Eq. (48), one sees that, because of the factor $2(f)^{1/2}/(1 + f)$, the addition of actual structural damping g_i may destabilize the system, particularly for systems where the aerodynamic damping g_A is small. The maximum

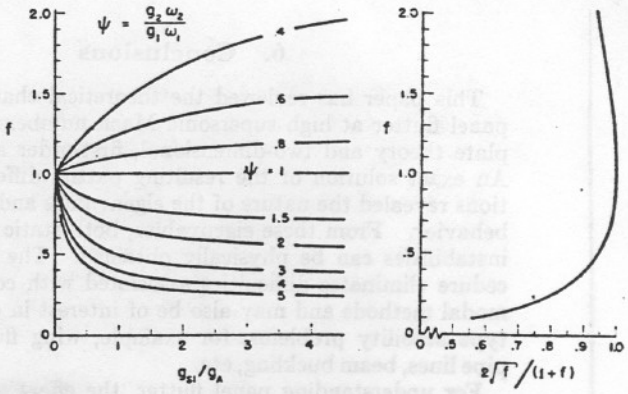

Fig. 16 Parameters for unequal damping.

amount of this destabilization possible depends solely on ψ and is given from the asymptotic values of f as

$$\frac{\lambda_F \text{ (with structural damping)}}{\lambda_F \text{ (no structural damping)}} \geqslant \frac{2(\psi)^{1/2}}{(1 + \psi)} \tag{55}$$

In the case of equal effective structural damping coefficients, $\psi = 1$, the system is always stabilized by the addition of actual structural damping g_i.†† The crucial role of the ratio ψ here is to be noted.

The previous theory was applied to a panel with $a/b = k = r_x = r_y = 0$. Two types of structural damping relationships were considered, namely, 1) $g_2 = g_1$ for which $\psi = 4$, and 2) $g_2 = \frac{1}{4}g_1$ for which $\psi = 1$. Figure 17 shows λ_F vs the actual structural damping g_1 present in the panel. At $g_A = 0.1$, the addition of actual structural damping $g_1 = 0.05$ will reduce λ_F from 274 to 258 for the $g_2 = g_1$ case, whereas there is a slight increase for the $g_2 = \frac{1}{4}g_1$ case. At $g_A = 1$, the destabilization for the $g_2 = g_1$ case is much less. These curves of λ_F vs g_1 clearly illustrate the typical "looping back" of the V-g curves of the standard flutter analysis used in industry. This "looping back" is seen to be a result of unequal effective structural damping coefficients.‡‡

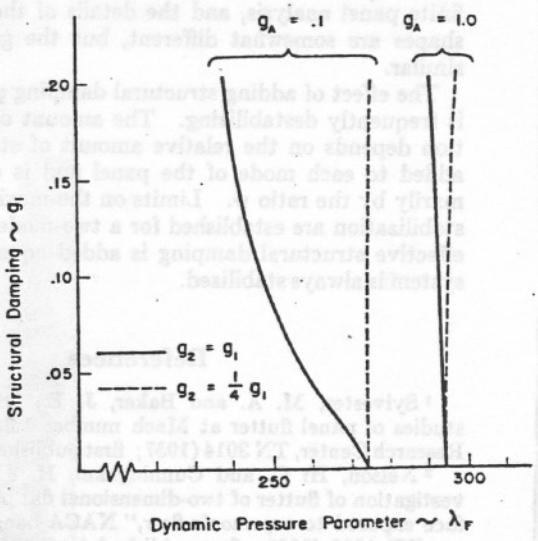

Fig. 17 Effects of structural damping ($a/b = k = r_x = r_y = 0$).

†† This destabilization occurring upon the addition of damping has been pointed out by Ziegler,[25] Bolotin,[9] Johns,[16] and others.

‡‡ Note that, for no aerodynamic or structural damping ($g_T = 0$), $\lambda_F = 274$ for these two-mode analyses rather than the exact value of $\lambda_F = 343$. A four-mode analysis should actually be done for numerical accuracy. Figure 17, however, does give the proper trends.

6. Conclusions

This paper has reviewed the theoretical characteristics of panel flutter at high supersonic Mach numbers, using linear plate theory and two-dimensional, first-order aerodynamics. An exact solution of the resulting partial differential equations revealed the nature of the eigenvalues and their general behavior. From these eigenvalues, both static and dynamic instabilities can be physically obtained. The solution procedure eliminates difficulties associated with convergence of modal methods and may also be of interest in other similar-type stability problems, for example, wing flutter, flowing pipe lines, beam buckling, etc.

For understanding panel flutter, the effect of damping is important. At low values of g_T, panel flutter occurs at constant dynamic pressure q and has the appearance of standing waves. At high values of g_T (light, thin panels in dense air), panel flutter occurs at constant velocity V and has the appearance of traveling waves. The use of the "static air force approximation" is adequate in some ranges but inadequate in others, particularly if $\lambda = 0$. This $\lambda = 0$ condition merely implies that flutter occurs at constant velocity V rather than at constant dynamic pressure q and does not mean that the system is unstable for any airspeed.

For pure aspect ratio and pure elastic foundation, only dynamic-type instabilities are possible, but, with compressive forces r_x, r_y present, static-type instabilities (buckling) can also occur.

The effects of front and rear edge conditions on the plate tend to become unimportant for low aspect ratios and also for high aerodynamic damping g_T, where the resulting mode shapes begin to appear like traveling waves.

The flutter condition appears to set in sharply for two-dimensional panels at low values of damping g_T. For low aspect ratios and for high values of g_T, the flutter condition comes in more mildly.

Infinite panel, traveling wave analysis can be used to obtain an approximate idea of the flutter characteristics of low-aspect-ratio panels at high values of damping g_T. The traveling wave analysis gives lower flutter speeds than the finite panel analysis, and the details of the deflection mode shapes are somewhat different, but the general trends are similar.

The effect of adding structural damping g_i to a finite panel is frequently destabilizing. The amount of this destabilization depends on the relative amount of structural damping added to each mode of the panel and is characterized primarily by the ratio ψ. Limits on the maximum possible destabilization are established for a two-mode analysis. If the effective structural damping is added equally ($\psi = 1$), the system is always stabilized.

References

[1] Sylvester, M. A. and Baker, J. E., "Some experimental studies of panel flutter at Mach number 1.3," NACA Langley Research Center, TN 3914 (1957; first published December 1952).

[2] Nelson, H. C. and Cunningham, H. J., "Theoretical investigation of flutter of two-dimensional flat panels with one surface exposed to supersonic flow," NACA Langley Research Center, TR 1280 (1956; first published April 1955).

[3] Fung, Y. C., "On two-dimensional panel flutter," J. Aeronaut. Sci. 25, 145–160 (1958).

[4] Hedgepeth, J. M. "Flutter of rectangular simply supported panels at high supersonic speeds," J. Aeronaut. Sci. 24, 563–573 (1957).

[5] Movchan, A. A., "On vibrations of a plate moving in a [illegible]," NASA Republication 11-22-58 W (January 1959); transl. [illegible] Prikl. Mat. Mekh. 20, 211–222 (1956).

[6] Houbolt, J. C., *A Study of Several Aerothermoelastic Problems of Aircraft Structures*, Mitteilungen Aus Institut fur Flugzeugstatik und Leichtbau, Nr. 5 (Verlag Leeman, Zurich, 1958).

[7] Guy, L. D. and Dixon, S. C., "A critical review of experiment and theory for flutter of aerodynamically heated panels," *Symposium on Dynamics of Manned Lifting Planetary Entry* (John Wiley & Sons Inc., New York, 1963), pp. 568–595.

[8] Voss, H. M., "The effect of an external supersonic flow on the vibrations of thin cylindrical shells," J. Aerospace Sci. 28, 945–956 (1961).

[9] Bolotin, V. V., *Nonconservative Problems of the Theory of Elastic Stability* (The Macmillan Co., New York, 1963).

[10] Fung, Y. C., "Some recent contributions to panel flutter research," AIAA J. 1, 898–909 (1963).

[11] Dowell, E. H. and Voss, H. M. "Experimental and theoretical panel flutter studies in the Mach number range 1.0 to 5.0," AIAA J. 3, 2292–2304 (1965).

[12] Fralich, R. W., "Postbuckling effects on the flutter of simply supported rectangular panels at supersonic speeds," NASA Langley Research Center, TN D-1615 (1963).

[13] Cunningham, H. J., "Analysis of the flutter of flat rectangular panels on the basis of exact three-dimensional, linearlized supersonic potential flow," AIAA J. 1, 1795–1801 (1963).

[14] Bohon, H. L. and Dixon, S. C., "Some recent developments in flutter of flat panels," J. Aircraft 1, 280–288 (1964).

[15] Fung, Y. C., "A summary of the theories and experiments on panel flutter," Guggenheim Aeronautical Lab., California Institute of Technology, Air Force Office of Scientific Research TN 60-224 (May 1960).

[16] Johns, D. J., "The present status of panel flutter," AGARD Rept. 484 (1964).

[17] Kordes, E. E., Tuovila, W. J., and Guy, L. D., "Flutt[illegible] search on skin panels," NASA Langley Research Center. TN D-451 (1960).

[18] Shirk, M. H. and Olsen, J. J., "Recent panel flutter research and applications," AGARD Rept. 475 (1963).

[19] Dugundji, J., "Theoretical considerations of panel flutter at high supersonic Mach numbers," Massachusetts Institute of Technology, Aeroelastic and Structures Research Lab. TR 134-1, Air Force Office of Scientific Research 65-1907 (August 1965).

[20] Ashley, H. and Zartarian, G., "Piston theory—a new aerodynamic tool for the aeroelastician," J. Aeronaut. Sci. 23, 1109–1118 (1956).

[21] Dugundji, J. and Ghareeb, N., "Pure bending flutter of a swept wing in a high-density, low speed flow," AIAA J. 3, 1126–1133 (1965).

[22] Movchan, A. I. and Movchan, A. A., "Traveling waves in the supersonic flutter problem of panels of finite length," *Proceedings of the International Council of Aerospace Sciences, Third Congress* (Spartan Books Inc., Washington, D. C., 1964), pp. 723–735.

[23] Movchan, A. A., "Behavior of complex eigenvalues in the problem of panel flutter," Acad. Sci. U.S.S.R., Inst. Mech., Inzh. Sbornik 27, 70–76 (1960).

[24] Dowell, E., "The flutter of very low aspect ratio panels," Massachusetts Institute of Technology, Aeroelastic and Structures Research Lab. TR 112-2, Air Force Office of Scientific Research 64-1723 (July 1964).

[25] Ziegler, H., "On the concept of elastic stability," *Advances in Applied Mechanics* (Academic Press Inc., New York, 1956), Vol. 4, pp. 351–403.